Fault Monitoring and Fault Recovery Control for Position Moored Tanker

Fang, Shaoji; Blanke, Mogens

Published in:
International Journal of Applied Mathematics and Computer Science

Link to article, DOI:
10.2478/v10006-011-0035-9

Publication date:
2011

Document Version
Early version, also known as pre-print

Int. J. Appl. Math. Comput. Sci., , Vol. , No. , –
DOI:

amcs

FAULT MONITORING AND FAULT RECOVERY CONTROL FOR POSITION MOORED TANKER

SHAOJI FANG [*], MOGENS BLANKE [**,*]

[*] Centre for Ships and Ocean Structures, Norwegian University of Science and Technology, NO 7491 Trondheim, Norway.
e-mail: shaoji.fang@ntnu.no

[**] Automation and Control Group, Department of Electrical Engineering, Technical University of Denmark, DK 2800 Kgs Lyngby, Denmark. e-mail: mb@elektro.dtu.dk

This paper addresses fault tolerant control for position mooring of a shuttle tanker operating in the North Sea. A complete framework for fault diagnosis is presented but the loss of a sub-sea mooring line buoyancy element is given particular attention, since this fault could lead to mooring line breakage and a high-risk abortion of an oil-loading operation. With significant drift forces from waves, non-Gaussian elements dominate forces and the residuals designed for fault diagnosis. Hypothesis testing need be designed using dedicated change detection for the type of distribution encountered. In addition to dedicated diagnosis, an optimal position algorithm is proposed to accommodate buoyancy element failure and keep the mooring system in a safe state. Furthermore, even in the case of line breakage, this optimal position strategy could be utilised to avoid breakage of a second mooring line. Properties of detection and fault-tolerant control are demonstrated by high fidelity simulations.

Keywords: Fault Diagnosis, Fault-tolerant Control, Position Mooring, Change Detection, Optimal Position Control, Non Gaussian Detection.

1. Introduction

With oil and gas exploration going into deeper waters and harsher environments, position mooring systems (PM) encounter more challenges with respect to mechanical reliability, automatic control and associated safety aspects. For thruster assisted position mooring, the main objective is to maintain the vessel's position within a limited region and keep the vessel at the desired heading such that the external environmental load is minimised. In extreme weather, the main objective changes to ensure that mooring lines avoid breakage. Related literatures include (Strand *et al*., 1998), (Aamo and Fossen, 2001), (Nguyen and Sørensen, 2007), (Berntsen *et al*., 2008a).

Safety of dynamic positioning is a prime concern in the marine industry and regulations are enforced to prevent faults in equipment to cause accidents with the system ((DNV, 2008b)). In position mooring system, accident limit status must be analysed in case of the line breakage or the loss of one or more mooring line buoyancy elements (MLBE). Such analysis is based on the reliability of mechanical structures, and studies of the sensitivity to extreme values and associated risk for fatigue damage or line breakage with the loads from environment ((Gao and Moan, 2007)). Recently, automatic control for safety has received increased attention in marine research. (Berntsen *et al*., 2006) proposed an nonlinear controller based on a structural reliability index to prevent the mooring line from getting into a low reliability zone. This algorithm mainly considered the safety status with structural reliability index. (Nguyen and Sørensen, 2009) treated a switching controller for thruster-assisted position mooring. This algorithm detected the change of varying environment characteristics and switched the controller to prevent mooring line breakage. Systematic fault tolerant control was studied for the station keeping of a marine vessel by (Blanke, 2005) and a structure-graph approach for fault diagnosis and control reconfiguration was validated by sea tests. (Nguyen and Sørensen, 2007) extended this study to the position mooring case and suggested an off-line fault accommodation design based on switching between different pre-determined controllers. Mooring line buoyancy elements were not considered in these previous studies.

The purpose of this paper is to widen fault tolerant control design for position mooring systems to include

loss of mooring line buoyancy elements and strengthen the fault tolerant control strategy in the case of mooring line breakage. Investigating control system topology by structure-graph analysis, diagnosis system design is extended to include buoyancy elements on mooring lines. Residuals are demonstrated to be non-Gaussian, due to the nature of drift forces from waves, and a dedicated change detection and hypothesis test is designed for the particular distributions. Fault accommodation is suggested to be done by a novel algorithm that is shown optimal in avoiding mooring line breakage. The safety status of a mooring line is evaluated against the critical value of mooring line tension for the fault-accommodating control and it is illustrated, by simulations, how the optimal position algorithm is activated and prevents mooring line tension from exceeding the critical value after the loss of a buoyancy element.

The remainder of this paper is organised as follows. Section 2 addresses modeling of the position moored vessel. Section 3 presents fault diagnosis and change detection. The optimal position algorithm in fault accommodation is presented at section 4. The proposed algorithm is validated by simulations in Section 5 and conclusions are drawn in section 6.

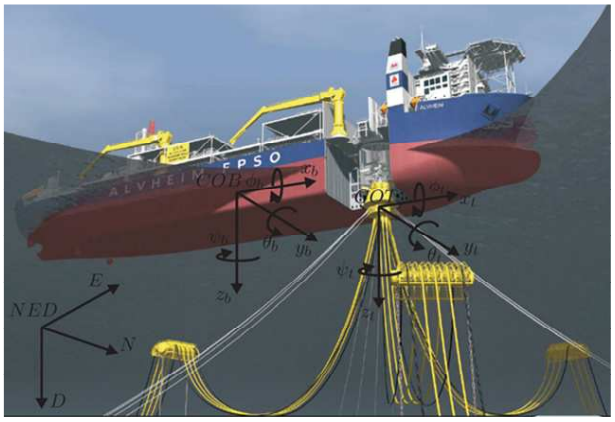

Fig. 1. Typical Position Mooring System

2. System Modeling

The purpose of the modeling is to obtain information to design fault detection and isolation (FDI) modules for essential faults and to give the prerequisites for the control reconfiguration design when the faults occur.

The basic configuration of position mooring system is shown in Fig. 2 according to the equipment demand of DYNPOS-AUTR class DP (DNV, 2008a), which is the most reliable system configuration according to the DNV classes, shown in Table 1. There are redundant thrusters, three position measurement systems (two GPS and one hydro-acoustic position unit (HPS)), two wind sensors, three gyro compasses and three vertical reference sensors (VRS). The relative velocity through water is measured by the ship's log and inertial measurement unit (IMU). Meantime, the mooring line tensions are monitored by tension measurement equipment (TME).

Table 1. Sensor Requirement of different DP classification

Sensor Number	AUTS	AUT	AUTR
N_{pos}	1	2	3
N_{wind}	1	1	2
N_{gyro}	1	1	3
N_{vrs}	1	1	3

Table 2 shows the list of symbols and the block diagram in Fig. 2 illustrates the topology of function blocks in a position mooring system. A typical position mooring system is shown in Fig. 1, along with two reference frames: the Earth fixed frame (EFF) and body fixed frame (BFF) with the origin located at the centre of the turret (COT), where all the mooring lines are attached to the vessel.

Table 2. List of symbols

symbol	Explanation
h_1, h_2, h_3	yaw measurements
$\psi, \dot{\psi}$	yaw angle and yaw rate
$\mathbf{p}_{G1}, \mathbf{p}_{G2}, \mathbf{p}_{H1}$	position measurements in EFF
$\mathbf{p}, \dot{\mathbf{p}}$	vessel position and velocity in EFF
$\mathbf{q}_1, \mathbf{q}_2, \mathbf{q}_3$	vertical reference measurements
z, ϕ, θ	vessel heave, roll and pitch
$\mathbf{w}_{m1}, \mathbf{w}_{m2}, \mathbf{c}_m$	wind and current measurements
$\mathbf{v}_w, \mathbf{v}_c$	wind and current velocity
$\mathbf{T}_{mbi}$	mooring line tension
$\mathbf{T}_{moi}$	MLBE force
$\mathbf{T}_{momi}$	mooring line tension measurement
$\mathbf{v}$	vessel velocity in BFF
$\mathbf{v}_m$	velocity measurement in BFF
$u_1, u_2, \ldots u_k$	thruster input
T_1, T_2, T_3	thruster force

In structural analysis, the model of a system is considered as a set of constraints $\mathbf{C} = \{a_1, \ldots, a_i, c_1, \ldots c_i, d_1, \ldots, d_i, m_1, \ldots, m_i\}$ that are applied to a set of variables $\mathbf{X} = X \cup K$. X denotes the set of unknown variables, $K = K_i \cup K_m$ known variables: measurements (K_m), control input (K_i) etc. Variables are constrained by the physical laws applied to a particular unit. a_i denotes the constraint of thruster input, c_i denotes the algebraic constraint, d_i denotes the differential constraint, m_i are the measurements. With three thrusters and n mooring lines, the constrains and variables for the PM are:

$$a_1: \quad T_1 = \quad g_t(u_1, u_2, \ldots, u_k)$$
$$a_2: \quad T_2 = \quad g_l(u_1, u_2, \ldots, u_k)$$

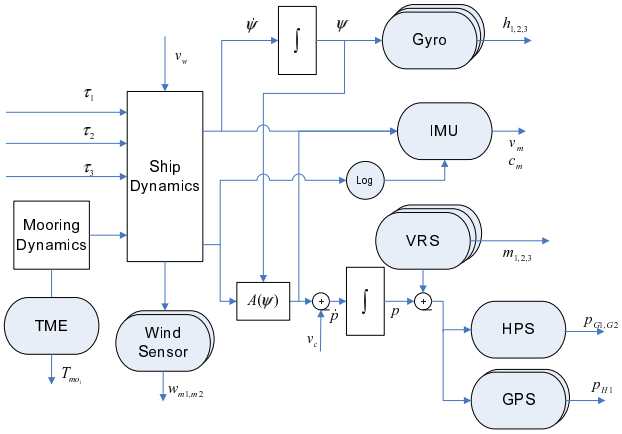

Fig. 2. Ship Configuration

$$
\begin{aligned}
a_3: \quad & T_3 = && g_l(u_1, u_2, \ldots, u_k)\\
c_1: \quad & \mathbf{M}\dot{\mathbf{v}} = && \mathbf{H}_{xy}\mathbf{T}[T_1, T_2, T_3]^\top + [g_w^x(v_w)\\
& && g_w^y(v_w)]^\top + \sum_{j=1}^{n} \mathbf{A}_{mo}^{xy}(\mathbf{p}, \psi)\\
& && \mathbf{T}_{moi}^{xy}(\mathbf{T}_{moi}) - \mathbf{D}[\mathbf{v} \quad \dot{\psi}]^\top\\
c_2: \quad & I\ddot{\psi} = && \mathbf{H}_{\psi}\mathbf{T}[T_1, T_2, T_3]^\top + g_w^{\psi}(v_w)\\
& && + \sum_{j=1}^{n} \mathbf{A}_{mo}^{\psi}(\mathbf{p}, \psi)\mathbf{T}_{moi}^{\psi}(\mathbf{T}_{moi})\\
c_3: \quad & \dot{\mathbf{p}} = && \mathbf{A}_{ve}(\psi)\mathbf{v} + \mathbf{v}_c\\
c_4: \quad & \mathbf{p}_{G1} = && \mathbf{p} + \mathbf{R}(\phi, \theta, \psi)\mathbf{l}_{G1}\\
c_5: \quad & \mathbf{p}_{G2} = && \mathbf{p} + \mathbf{R}(\phi, \theta, \psi)\mathbf{l}_{G2}\\
c_6: \quad & \mathbf{p}_{H1} = && \mathbf{p} + \mathbf{R}(\phi, \theta, \psi)\mathbf{l}_{H1}\\
c_{2i+5}: \quad & \mathbf{T}_{moi} = && g_{mo}(\mathbf{p}, \psi, \mathbf{T}_{mbi})\\
c_{2i+6}: \quad & \mathbf{T}_{mbi} = && g_{mb}(\mathbf{p}, \psi)\\
d_1: \quad & \dot{\mathbf{v}} = && \frac{\partial}{\partial t}\mathbf{v}\\
d_2: \quad & \dot{\mathbf{p}} = && \frac{\partial}{\partial t}\mathbf{p}\\
d_3: \quad & \dot{\psi} = && \frac{\partial}{\partial t}\psi\\
d_4: \quad & \ddot{\psi} = && \frac{\partial}{\partial t}\dot{\psi}\\
m_1..m_3: \quad & h_{1..3} = && \psi\\
m_4: \quad & \mathbf{p}_{G1}^m = && \mathbf{p}_{G1}\\
m_5: \quad & \mathbf{p}_{G2}^m = && \mathbf{p}_{G2}\\
m_6: \quad & \mathbf{p}_{H1}^m = && \mathbf{p}_{H1}\\
m_7..m_9: \quad & \mathbf{q}_{1..3} = && [z \quad \phi \quad \theta]\\
m_{10}: \quad & \mathbf{v}_m = && \mathbf{v}\\
m_{11,12}: \quad & \mathbf{w}_{m1,m2} = && \mathbf{v}_w\\
m_{13}: \quad & \mathbf{c}_m = && \mathbf{v}_c\\
& && \\
m_{13+i}: \quad & \mathbf{T}_{momi} = && \mathbf{T}_{moi},
\end{aligned}
$$

where $\mathbf{M}$ is mass matrix including added mass, $\mathbf{D}$ is damping matrix, I is inertia moment for yaw, $\mathbf{T}$ is thruster configuration matrix, $\mathbf{H}_{xy}$ is projection matrix for surge and sway, $\mathbf{H}_{\psi}$ is that for yaw, $\mathbf{A}_{mo}^{xy}, \mathbf{A}_{mo}^{\psi}$ is transformation matrix for horizontal mooring line tension from the Earth fixed frame to the body fixed frame, $\mathbf{A}_{ve}(\psi)$ is a transformation matrix for vessel velocity from the Earth fixed frame to body fixed frame, $\mathbf{R}(\phi, \theta, \psi)$ is transformation matrix from the location of position reference system to the vessel coordinate origin, and $g_w^x(v_w)$, $g_w^y(v_w)$,$g_w^{\psi}(v_w)$ are the wind force in surge, sway and yaw directions.

Categorising into sets of unknown variables, input variables and measurement variables, the variables on the above constraints can be separated as:

$$
\begin{aligned}
X &= \{T_1, T_2, T_3, \mathbf{T}_{mbi}, \mathbf{T}_{moi}, \mathbf{p}_{G1}, \mathbf{p}_{G2},\\
&\quad \mathbf{p}_{H1}, \mathbf{v}, \dot{\mathbf{v}}, \psi, \dot{\psi}, \ddot{\psi}, , \mathbf{p}, \dot{\mathbf{p}}, \theta, \phi, \mathbf{v}_c, \mathbf{v}_w\}\\
K_i &= \{u_1, u_2, \ldots, u_k\}\\
K_m &= \{h_1, h_2, h_3, \mathbf{p}_{G1}^m, \mathbf{p}_{G2}^m, \mathbf{p}_{H1}^m, \mathbf{q}_1,\\
&\quad \mathbf{q}_2, \mathbf{q}_3, \mathbf{v}_m, , \mathbf{w}_{m1}, \mathbf{w}_{m2}, \mathbf{c}_m, \mathbf{T}_{momi}\}.
\end{aligned}
$$

The above modeling of the moored system does not include bifurcations that could occur when second order wave forces interact with the dynamics of a moored system. Analytical conditions for boundaries where static and dynamic loss of stability occurs when a bifurcation boundary is crossed were derived by (Garza-Rios and Bernitsas, 1996). The modeling here presents the normal behaviour, and diagnostic algorithms are designed to detect deviation from normal (Blanke *et al.*, 2006), hence the onset of a bifurcation in the motion of the moored vessel could be detected and counteracted by thruster assisted position control.

3. Fault Diagnosis and Change detection

3.1. Analysis of Structure. The structure graph approach is usually employed to obtain the system analytical redundancy relations for FDI. With this technique, the functional relations with measured and control variables need not be explicitly stated. SaTool is a software developed for this technique and a structure graph can be created based on implicit nonlinear constraints (Blanke, 2005).

The structural analysis finds the over-determined subsystem and a set of $10 + i$ parity relations where i is the number of mooring lines. These parity relations can be used as residual generators for fault detection in general in the system. A deviation from normal of a constraint, i.e. a fault, will affect a parity relation if this parity relation is constructed using the constraint. Considering mooring

line faults, the result is $2+i$ such relations:

$$\begin{aligned}
r_1 &= c_1(a_1(u_1), a_2(u_2), c_6(m_3(h_3), m_9(\mathbf{q}_3), \\
&\quad m_6(\mathbf{p}^m_{H1})), m_3(h_3), c_{2i+5}(c_6(m_3(h_3), m_9(\mathbf{q}_3), \\
&\quad m_6(\mathbf{p}^m_{H1})), m_3(h_3), c_{2i+6}(c_6(m_3(h_3), m_9(\mathbf{q}_3), \\
&\quad m_6(\mathbf{p}^m_{H1})), m_3(h_3))), m_{12}(\mathbf{w}_{m2}), m_{10}(\mathbf{v}_m), \\
&\quad d_3(m_3(h_3))) \\
r_2 &= c_2(a_3(u_3), c_6(m_3(h_3), m_9(\mathbf{q}_3), m_6(\mathbf{p}^m_{H1})), \\
&\quad m_3(h_3), c_{2i+5}(c_6(m_3(h_3), m_9(\mathbf{q}_3), \\
&\quad m_6(\mathbf{p}^m_{H1})), m_3(h_3), c_{2i+6}(c_6(m_3(h_3), \\
&\quad m_9(\mathbf{q}_3), m_6(\mathbf{p}^m_{H1})), m_3(h_3))), m_{12}(\mathbf{w}_{m2}), \\
&\quad m_{10}(\mathbf{v}_m), d_3(m_3(h_3)), d_4(d_3(m_3(h_3)))) \\
r_{5+i} &= m_{13+i}(\mathbf{T}_{momi}, c_{2i+5}(c_6(m_3(h_3), m_9(\mathbf{q}_3), \\
&\quad m_6(\mathbf{p}^m_{H1})), m_3(h_3), c_{2i+6}(c_6(m_3(h_3), \\
&\quad m_9(\mathbf{q}_3), m_6(\mathbf{p}^m_{H1})), m_3(h_3)))).
\end{aligned}$$

If a fault affects residual vector, the fault is structurally detectable. If a particular fault has a unique pattern in the residual vector's elements, it is structurally isolable. In the presence of only one fault, structurally isolable constraints are $(d_2, m_1, m_2, m_3, m_7, m_8, m_9, m_{10}, m_{11}, m_{12}, m_{13+i})$. The rest are only detectable.

Considering a fault on a mooring line, the dependency matrix is shown in Table 3. Violations of constraints c_{2i+5} and c_{2i+6} are only detectable but their residual vectors are unique from those of the other cases. This shows that the fault on the buoy can be distinguished from the fault of the mooring line itself. The constrains m_{13+i} are isolable and thus the fault on the tension measurement equipment can be distinguished from the fault on the mooring line, if only a single fault is present. When faults are only group-wise isolable, active fault diagnosis techniques could be applied. This was pursued for a position moored tanker without buoyancy elements in (Nguyen and Blanke, 2010).

Table 3. Dependency Matrix

	c_{2i+5}	c_{2i+6}	m_{13+i}
r_1	1	1	0
r_2	1	1	0
r_{5+i}	1	1	1

3.2. Change Detection. After design of the residual generators, hypothesis testing needs to be designed to detect the change of the residual. For violation of constraints c_{2i+5}, c_{2i+6}, changes will be structurally visible on residuals r_1, r_2 and r_{5+i}.

The design intention of the mooring line buoyancy element (MLBE) is to reduce the static force and dynamic motion of the mooring system (Mavrakos *et al.*, 1996). Buoyancy elements need be designed suitably, otherwise adverse effects could occur. The loss of a buoyancy element would cause deviation of static forces on the mooring line and a similar effect would also occur in case of the line breakage. This deviation is reflected on the residuals r_{5+i} while the acceleration deviation of PM is reflected on the residuals r_1 and r_2. The detection algorithm of the static force deviation in r_{5+i} could be found in (Nguyen *et al.*, 2007) with a fault that one mooring line is broken, while the focus of the change detection here is for the deviation of residual r_1 and r_2 in the case that a buoyancy element is lost.

However, all of these residuals are non-Gaussian distributed due to nonlinear vessel dynamics and nature of wave drift forces. First order wave forces will generally give Gaussian distributions and the slowly varying drift forces can be calculated to give Rayleigh distributed forces, if one just assumes that forces arise as the amplitude of a sum of gaussian elements. More accurate assessment of the distribution of forces on a moored tanker was the subject of studies including (Wang and Xu, 2008) where forces and moments affecting an FPSO were computed by the near-field method based on direct pressure integration. (Wang and Tan, 2008) modeled the response of a moored vessel excited by slowly varying non-Gaussian wave drift forces as a continuous Markov process. (Næss, 1986) studied the statistical distribution of slowly varying drift forces and moments. The distribution of these forces and moments enter into the expressions of the residual we generate for fault diagnosis, but since residual generation involves dynamics and filtering by the residual generator, amplitude distribution of residuals are not the same as the amplitude distributions of wave drift forces and moments, although they off course are related. The problem of finding the distribution of residuals by analytical means is not within the scope of the present paper. Instead we turn to simulations and an approximation to observed distributions with and without faults being present.

The distribution of residual r_1 is shown in Fig. 3 that also shows an approximating Rayleigh distribution. The approximation is not a perfect match to the residual as obtained from simulations but for detection of change, it is clearly better than commonly applied detection algorithms for Gaussian distributed residuals (Kay, 1998).

From Fig. 3, the mean value of the residual r_1 is shifted away from zero, both with and without faults being present. A shifted Rayleigh density function replicates this behaviour. Considering that relationship between the variance of Rayleigh-distributed signal σ_R and the variance of underlying Gaussian signal σ is $\sigma_R^2 = (2-\frac{\pi}{2})\sigma^2$, the shifted Rayleigh density function is expressed as:

$$p(z(k)) = \frac{(4-\pi)(z(k)-\mu_R+\frac{\sqrt{\sigma_R^2\pi}}{\sqrt{4-\pi}})}{2\sigma_R^2}$$

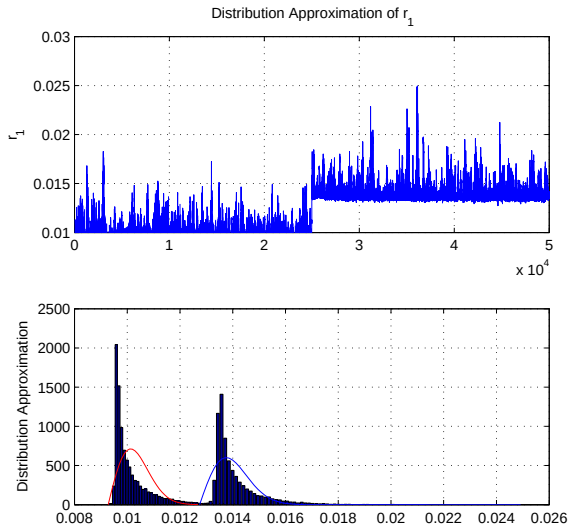

Fig. 3. Distribution Approximation of r_1

$$\exp[-\frac{(\sqrt{4-\pi}(z(k)-\mu_R)+\sqrt{\sigma_R^2\pi})^2}{4\sigma_R^2}]$$

$$\text{for} \qquad z(k) \geq \mu_R - \frac{\sqrt{\sigma_R^2\pi}}{\sqrt{4-\pi}},$$

where σ_R^2 is the variance of the Rayleigh distributed signal and μ_R is its mean value.

Detection of a change is suitably done using a Rao-test (Kay, 1998), which is the suitable detector for the mean value change in a Non-Gaussian noise. The hypothesis for this case is therefore given by:

$$\begin{aligned} H_0 &: \quad z(k) = \mu_0 + w(k) \qquad k = 0, 1, \ldots, N-1 \\ H_1 &: \quad z(k) = \mu_1 + w(k) \qquad k = 0, 1, \ldots, N-1. \end{aligned}$$

where the signal $w(k)$ is Rayleigh, μ_0 and μ_1 are the mean values before and after a change. Then the test statistics for the Rao-Test can be written as:

$$T_R(z) = \frac{(\frac{\partial \text{In}(p(z,\mu_R))}{\partial \mu_R}|_{\mu_R=\hat{\mu}})^2}{I(\hat{\mu})} > \gamma \tag{1}$$

where $\hat{\mu}$ is an estimate of the signal's mean value, $I(\hat{\mu})$ is the Fisher information and the probability density function $p(z, \mu_R)$ is:

$$p(z,\mu_R) = \frac{(4-\pi)^N (z(k)-\mu_R+\frac{\sqrt{\sigma_R^2\pi}}{\sqrt{4-\pi}})^N}{2^N \sigma_R^{2N}}$$
$$\exp(-\frac{\sum_{k=0}^{N-1}(\sqrt{4-\pi}(z(k)-\mu_R)+\sqrt{\sigma_R^2\pi})^2}{4\sigma_R^2})$$

The partial derivative of the logarithm of probability density function is found as:

$$\frac{\partial \text{In}(p(z,\mu_R))}{\partial \mu_R} = \frac{4-\pi}{2\sigma_R^2}\sum_{n=0}^{N-1}(z(k)-\mu_R+$$
$$\sqrt{\frac{\pi\sigma_R^2}{4-\pi}}) - \frac{2\sigma_R^2}{4-\pi}\sum_{n=0}^{N-1}\frac{1}{z(k)-\mu_R+\sqrt{\frac{\pi\sigma_R^2}{4-\pi}}} \tag{2}$$

The Fisher information with the Rayleigh distribution is found to be:

$$I(\mu_R) = \frac{N(4-\pi)}{2\sigma_R^2}\sqrt{\frac{\pi\sigma_R^2}{4-\pi}} + \frac{2\sigma_R^2}{(4-\pi)^2}$$
$$\sum_{n=0}^{N-1}\frac{1}{(\sqrt{4-\pi}(z(k)-\mu_R)+\sqrt{\pi\sigma_R^2})^2} \tag{3}$$

where μ_R is estimated online as $\mu_R = \hat{\mu}$ and σ_R is assumed to be unchanged. Finally the test statistics $T_R(z)$ can be deducted based on Equation (1) with Equations (2) and (3).

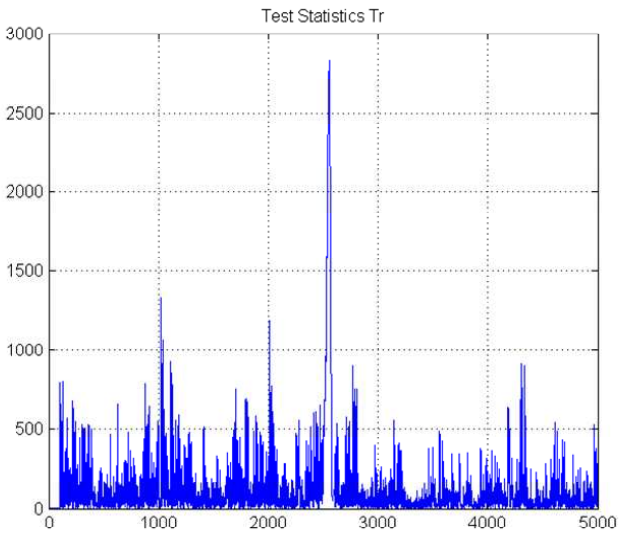

Fig. 4. Time history of test statistics

The above detector derived from Equation (1)-(3) is only available for the data larger than zero and the Rayleigh density function is shifted to have the mean value μ_R. Then the data need to satisfy:

$$\epsilon(k) = \max(z(k) - \mu_R + \sqrt{\frac{\sigma_R^2\pi}{4-\pi}}, 0). \tag{4}$$

In order to be able to use the same threshold for all tests, data are normalised and the result of the test statistics is shown in Fig. 4.

As shown in Fig. 4, test statistics is quite fluctuating in the first 2500 s while the system comes to a steady state.

The loss of one buoy is simulated to happen at time 2500 s and the event is rapidly detected.

The change detection method applied here is based on the residuals generated in symbolic form through structural analysis, and subsequently deduced in analytical form using the system constraints. Some faults will not be isolable through this approach but active fault isolation can help isolate faults by applying dedicated test signals on thrusters once a fault has been detected. Active fault diagnosis was analysed for Gaussian residuals by (Poulsen and Niemann, 2008) and references herein. The structural conditions were obtained by (Blanke and Staroswiecki, 2006) and a detailed design and test on a position moored tanker was presented in (Nguyen and Blanke, 2010) making use of active diagnosis.

4. Fault Tolerant Control

4.1. Controller design. The control objective is to maintain the vessel's position in a limited region and keep the vessel at the desired heading such that the external environmental load is minimised. Another objective is to avoid line breakage and keep the mooring system at a safe state. An optimal position algorithm is designed to meet the second objective. For the controller design, it is common to use multi-variable PID control in PM systems with the structure:

$$\boldsymbol{\tau}_{thr} = -\mathbf{K}_i\mathbf{R}^T(\psi)\int \hat{\boldsymbol{\eta}}_e dt - \mathbf{K}_p\mathbf{R}^T(\psi)\hat{\boldsymbol{\eta}}_e - \mathbf{K}_d\hat{\boldsymbol{\nu}}_e \quad (4$$

where $\hat{\boldsymbol{\eta}}_e = \hat{\boldsymbol{\eta}} - \boldsymbol{\eta}_d$, $\hat{\boldsymbol{\nu}}_e = \hat{\boldsymbol{\nu}} - \boldsymbol{\nu}_d$ are the position and velocity errors; $\boldsymbol{\eta}_d$ and $\boldsymbol{\nu}_d$ the desired position and velocity vectors; $\mathbf{K}_d$, $\mathbf{K}_i$ and $\mathbf{K}_d \in \mathbb{R}^{3\times 3}$ are the non-negative controller gain matrices. ψ is the measured heading angle and $\mathbf{R}(\psi)$ is the rotation matrix from Body-fixed Frame to Earth-fixed Frame, which can be found in (Fossen, 2002) However, in case of certain faults, this controller can not provide sufficiently good control.

4.2. Optimal position chasing. To maintain all mooring lines at a safe state, an optimal position algorithm is proposed here. A position mooring system is restricted to a safety region, which is normally defined from considering the static mooring line tension (Nguyen and Sørensen, 2007). A reliability index was also used to evaluate this region (Berntsen *et al.*, 2008a). This section proposes a new optimal position algorithm based on the mooring line tension for use in on-line fault-tolerant control.

First, a reference model is used for obtaining smooth transitions in the chasing of the optimal position set-point. This reference model refers to (Fossen, 2002) and it produces a smooth position reference which is the input to the position control law in Equation (5).

Optimal set-point is achieved through a quadratic object function based on each mooring line horizontal tension as:

$$L(T_{m1}, T_{m2}, \ldots, T_{mn}) = \sum_{i=1}^{n} \alpha_i T_{mi}^2 \qquad (6)$$

where T_{mi} is the ith horizontal mooring line tension and α_i a weighting factor. For the mooring system fixed on a turret, motion of a mooring line is shown in Fig. 5. The ith mooring line is fixed on the sea floor with an anchor at point (x_i^a, y_i^a). At the other end, the mooring line is connected to the turret at terminal point (TP) (x_{io}, y_{io}) and centre of the turret is at point (x_o, y_o). From the point (x_{io}, y_{io}) to the point (x_i, y_i), the terminal point moves with distance Δr and the direction β. Meanwhile, length of the mooring is changed from h_{io} to h_i and angle of the mooring in the Earth-fixed frame is changed from β_{io} to β_i. For the mooring system connected to a turret, the terminal point is assumed to be connected in the turret's centre and the body-fixed frame is set on the centre of the turret. Thus Δr also denotes the vessel's change in posi-

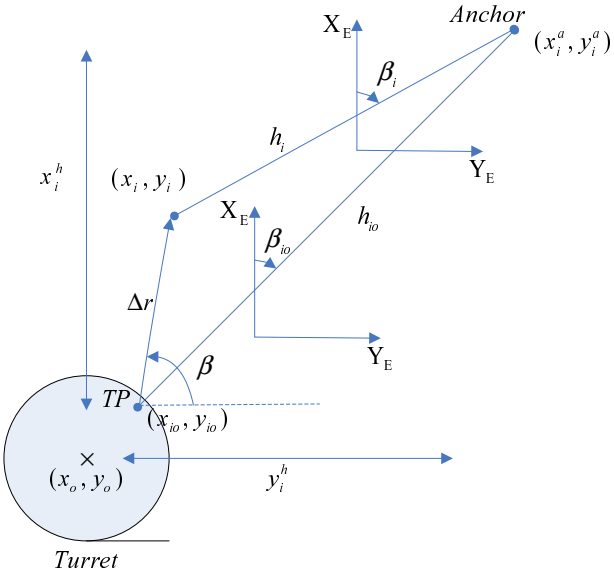

Fig. 5. Motion of one mooring line

The horizontal mooring line tension T_i at the point (x_i, y_i) can be expressed as a function of the in-plane increment of surface vessel position Δr and the direction β as:

$$\begin{aligned} T_i &= T_{oi} + c_i\Delta h = T_{oi} - c_i\Delta r\cos(90^\circ - \beta - \beta_{oi}) \\ &= T_{oi} - c_i\Delta r\sin(\beta + \beta_{io}), \end{aligned}$$

where T_{oi} is the tension in the working point (x_o, y_o) and c_i is the incremental stiffness tension at the present

instantaneous working point according to (Strand *et al.*, 1998).

The optimal position algorithm adjusts the optimal vessel set-point with the variation of the mooring line tensions. One application is that mooring lines lie in a zone where there is risk of breakage. Then evaluation for horizontal mooring line tension could be $T_{mi} = T_{ci} - T_i$ once the ith mooring line has a risk to be beyond the critical tension T_{ci}. Or the weighting coefficient w_i is adjusted to emphasise the importance of a certain mooring line. In the case of the faulty condition, for an example, lost MLBE and subsequent mooring line breakage, this algorithm is very useful. In addition, according to the regulation in the class society (DNV, 2008b), even the case that the mooring lines applied on the vessel are different, the safety of which can also utilise this approach. Thus with this algorithm, not only prevention of mooring line breakage can be analysed, but the control action is also used on-line to obtain safe behaviour in a real implementation.

For notation simplification, the object function of all mooring lines in a region of risk is:

$$\begin{aligned} L(T_{m1}, T_{m2}, \ldots, T_{mn}) &= \sum_{i=1}^{n} \alpha_i T_{mi}^2 \\ &= \sum_{i=1}^{n} \alpha_i (T_{ci} - T_i)^2 \end{aligned} \quad (7)$$

By solving the equations where the partial derivative of Equation (7) with respect to the optimal increment of the vessel position and the optimal direction of this increment are set to zero, the minimum value of the object function is hence identified. The optimal increment of vessel position Δr and the optimal direction of this increment β^o is found to be:

$$\begin{aligned} \Delta r &= \frac{K_{11}\sin\beta^o + K_{12}\cos\beta^o}{K_{21}\sin^2\beta^o + 2K_{22}\sin\beta^o\cos\beta^o + K_{23}\cos^2\beta^o} \\ \beta^o &= \mathrm{tg}^{-1}\frac{K_{11}K_{23} - K_{12}K_{22}}{K_{21}K_{12} - K_{11}K_{22}}, \end{aligned}$$

where:

$$\begin{aligned} K_{11} &= \alpha_1(T_{c1} - T_{o1})c_1\cos\beta_{1o} + \alpha_2(T_{c2} - T_{o2})c_2 \\ &\quad \cos\beta_{2o} + \cdots + \alpha_n(T_{cn} - T_{on})c_n\cos\beta_{no} \\ K_{12} &= \alpha_1(T_{c1} - T_{o1})c_1\sin\beta_{1o} + \alpha_2(T_{c2} - T_{o2})c_2 \\ &\quad \sin\beta_{2o} + \cdots + \alpha_n(T_{cn} - T_{on})c_n\sin\beta_{no} \\ K_{21} &= \alpha_1 c_1^2\cos^2\beta_{1o} + \alpha_2 c_2^2\cos^2\beta_{2o} + \ldots \\ &\quad + \alpha_n c_n^2\cos^2\beta_{no} \\ K_{22} &= \alpha_1 c_1^2\sin\beta_{1o}\cos\beta_{1o} + \alpha_2 c_2^2\sin\beta_{2o}\cos\beta_{2o} \\ &\quad + \cdots + \alpha_n c_n^2\sin\beta_{no}\cos\beta_{no} \\ K_{23} &= \alpha_1 c_1^2\sin^2\beta_{1o} + \alpha_2 c_2^2\sin^2\beta_{2o} + \cdots + \\ &\quad \alpha_n c_n^2\sin^2\beta_{no}. \end{aligned}$$

Finally in the general three-dimensional case, the updated vessel position and heading set-point become:

$$\eta = \eta_o + \Delta r[\cos\beta^o \quad \sin\beta^o \quad 0]^\top. \quad (8)$$

5. Simulation

The purpose of this simulation is to validate the proposed fault tolerant control strategy for the PM vessel subjected to loss of an MLBE and demonstrate that mooring line breakage is prevented.

5.1. Overview. The simulation is carried out using the Marine System Simulator (MSS) developed at the Norwegian University of Science and Technology (NTNU).

A turret-moored floating production, storage and offloading vessel model (FPSO) from the MSS library is used here. The turret mooring system consists of four mooring lines with buoys shown in Fig. 6. The mooring length is $L = 2250m$, the diameter is $D = 0.08m$, the cable density is $\rho_c = 5500kg/m^3$, the added mass coefficient $C_{mn} = 1.5$, the normal drag coefficient is $C_{dn} = 1$, the tangential drag coefficient is $C_{dt} = 0.3$. A buoy is connected at the position $s = 750m$ along un-stretched mooring line from the terminal point. The buoy is 8 $\times 10^4$ kg with the volume $V = 120m^3$. The added mass of the buoy is 5.8 $\times 10^4$ kg and the drag force coefficient is $C_{dx} = 0.7$. The working water depth is 1000 m and the mooring lines are simulated from finite element model with RIFLEX software (MARINTEK, 2003). Each mooring line consists of 300 finite elements. From the touch point to the buoy, 100 elements are made and there are 200 from the buoy to the terminal point.

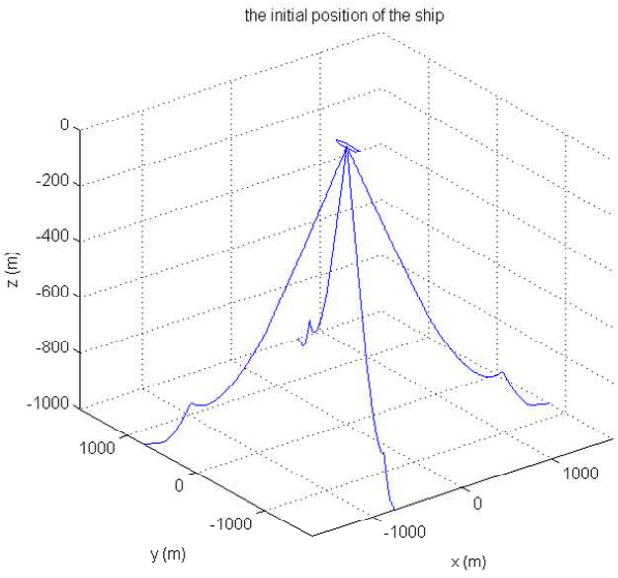

Fig. 6. Initial condition of simulation

For the external force, a JONSWAP wave spectrum is used with the significant wave height $H_s = 2m$ and the wave period $T_p = 5s$. The current is $v_c = 1m/s$ at the top and decreases to 0.2 m/s at the depth 500 m. At the bottom of sea floor, the current is 0 m/s. Wind speed is $v_w = 8m/s$ and the direction is 45 deg. The environmental simulation on the vessel refers to (Fossen, 2002) and the current profile simulation refers to (MARINTEK, 2003).

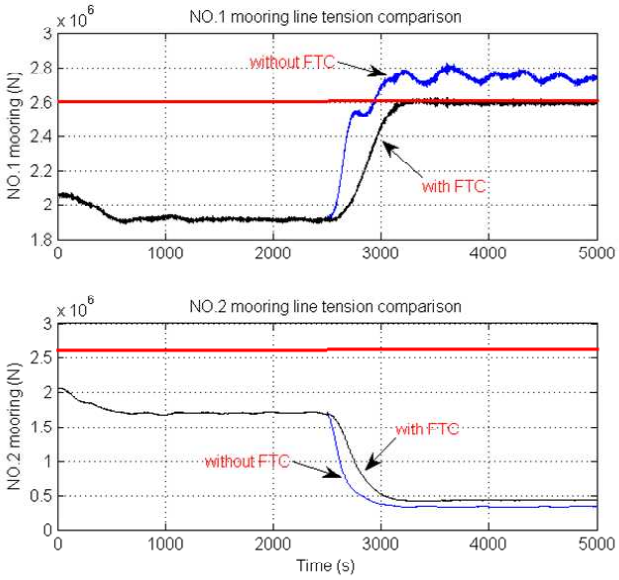

Fig. 7. No.1 and No.2 mooring line tension with line breakage

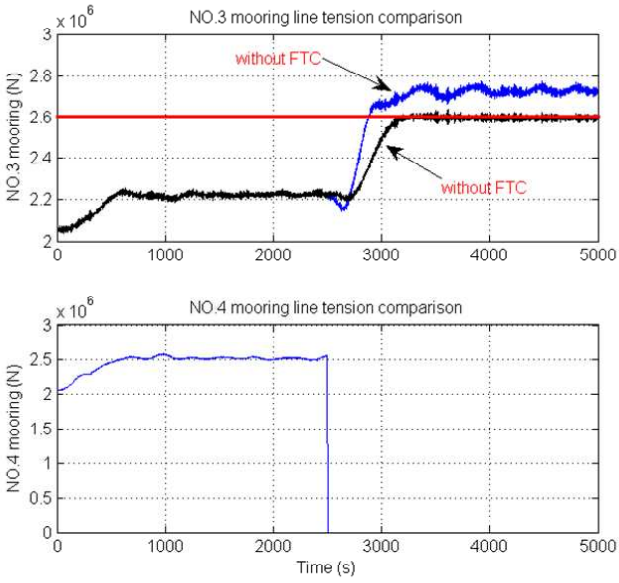

Fig. 8. No.3 and No.4 mooring line tension with line breakage

5.2. Simulation with line breakage. In the presence of strong sea current, the mooring line has a high risk of breaking if not adequately assisted by thrusters. (Nguyen *et al.*, 2007) recommended to evaluate the external environment and off-line determine a critical level of slowly-varying drift forces and switch to appropriate controls to compensate the increasing environmental forces according to change of environment. The PM is limited in the region evaluated by a certain critical position that did not consider the influence of current on the mooring lines. The optimal position algorithm proposed here utilise the mooring line tension for evaluation of external environmental effects and performs an online calculation of an optimal position to avoid line breakage.

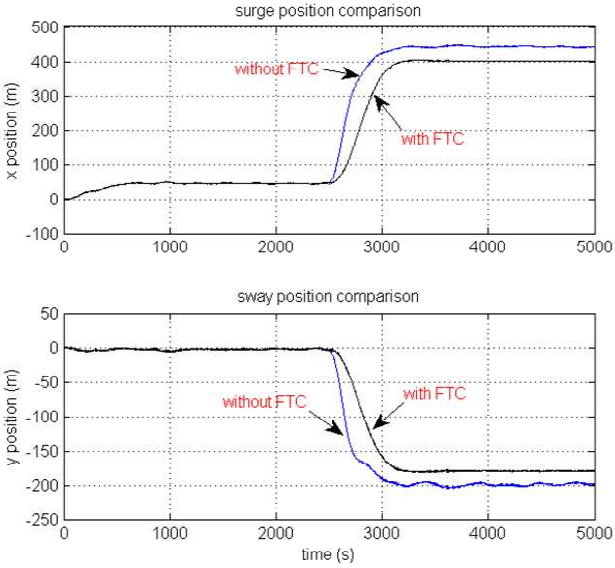

Fig. 9. The variation of position with line breakage

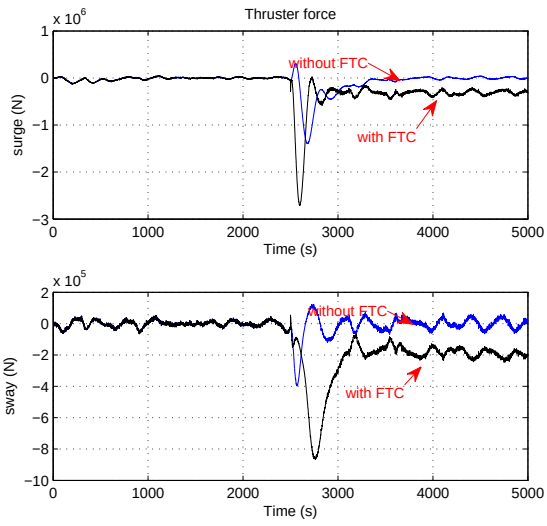

Fig. 10. Commanded thruster force with line breakage

If one of the mooring lines break, another equilib-

rium point will exist, depending on external forces. The new equilibrium has a high possibility of getting beyond the critical tension for other mooring lines, however, and in turn this could cause further breakage of lines. A simulation of an abrupt line breakage is shown in Figures 7 to 8 where number 4 mooring line encounters a breakage at $t = 2500s$. From Fig. 7 and 8, the no.1 and no.3 mooring line tensions rapidly afterwards get beyond the critical mooring line tension $T_m = 2.6e6$ N. This is avoided by the optimal position algorithm. With the optimal position algorithm, the NO.2 mooring line tension is higher than that of the case without the optimal position algorithm, but its value is kept below critical tension.

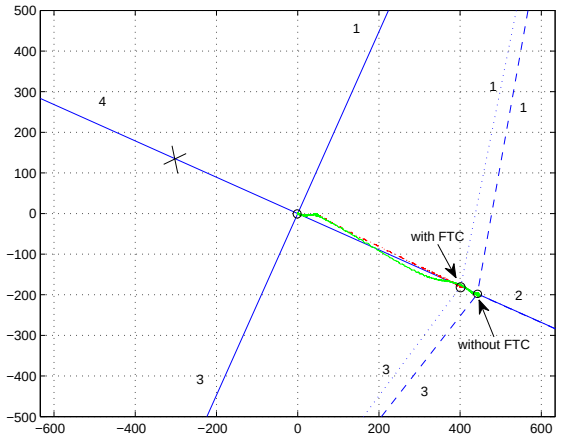

Fig. 11. Horizontal Motion with line breakage

Position deviation from the origin is shown in Figures 9 and 11 when line no. 4 breaks and the thruster force demand in Fig. 10. The thrusters compensate part of restoring force of mooring system with optimal position algorithm and the PM comes into an optimal set-point denoted 'with FTC'. There is a large transient in thruster force when the line breaks since the controller shortly has to compensate for the force component that disappeared. The thrusters attempt to compensate part of mooring system restoring force and then drive the PM to a new optimal point, will necessarily give rise to a transient. A rapid change in system dynamics over a short time, after the breakage, also has an effect.

The case was chosen to also illustrate two mooring lines getting beyond the critical tension almost simultaneously. The optimal position algorithm can handle this situation. This is an improvement from the first structural reliability based nonlinear controller by (Berntsen *et al.*, 2008b) that could handle only one critical mooring line.

It is a salient feature of the new algorithm that there is no limit to the number of mooring lines that can be handled by the optimal position algorithm although, according to the class regulation (DNV, 2008b), the PM system is only required to be fully operational with one mooring line breakage. This feature of the algorithm requires that sufficient thruster forces are available.

5.3. Simulation with lost MLBE. A buoy lost is another event where mooring lines could come beyond critical tension. A simulation with this event is shown in Fig. 12-14. In the simulation, No.2 mooring line tension increases after the buoy is lost at $t = 2500$ s and the mooring system comes into a new equilibrium where No.2 mooring line is still within safe range. The tension analysis for mooring line with MLBE must be done before employing the MLBE and thus in the structural view, the mooring line with or without buoy should be safe. However, the mooring line 4 tension increases to beyond its critical value with the loss of MLBE in NO.2 mooring line. Mooring lines 1 and 3 are not critical as their tensions are well below the limit.

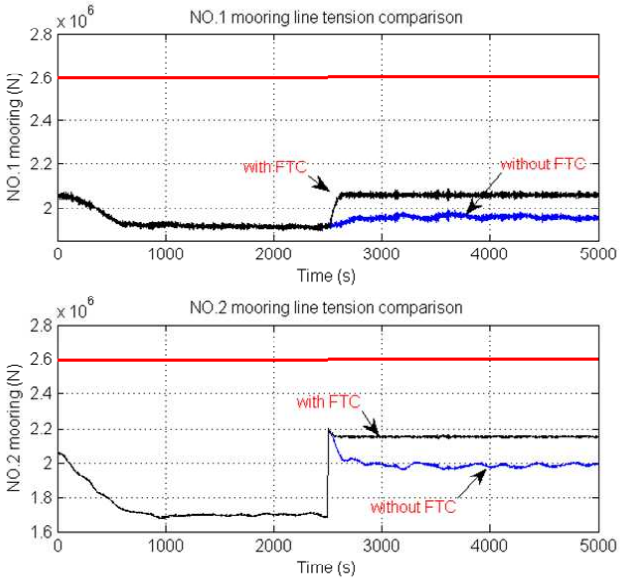

Fig. 12. No.1 and No.2 mooring line tension with lost MLBE

With the optimal position algorithm, PM moves to the optimal position shown in Fig. 14 after the loss of MLBE in NO.2 mooring line. Mooring line 4 comes close to critical tension, but the mooring system remains safe with all lines below critical tension. This algorithm could also be extended to simultaneous faults and protect PM for more than one mooring line in danger.

6. Conclusion

Fault tolerant control for position mooring was analysed in this paper with specific emphasis given to the case of loss of a mooring line buoyancy element and line breakage. Position mooring control was analysed with the dynamics of mooring line buoys attached. Structural analysis was employed to get residuals to detect changes that

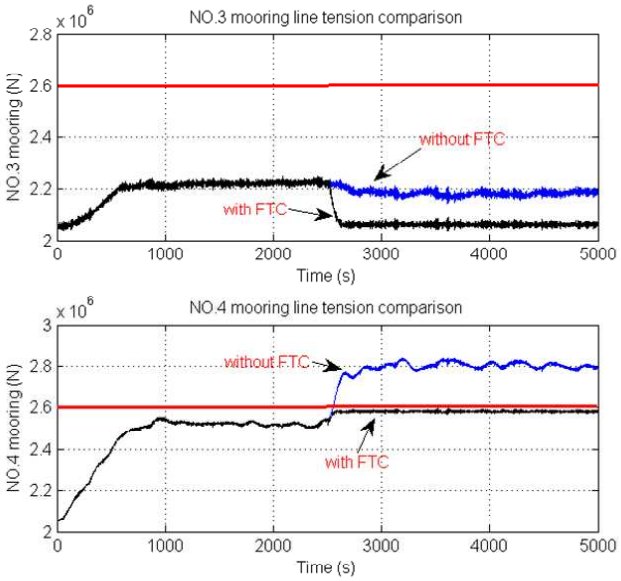

Fig. 13. No.3 and No.4 mooring line tension with lost MLBE

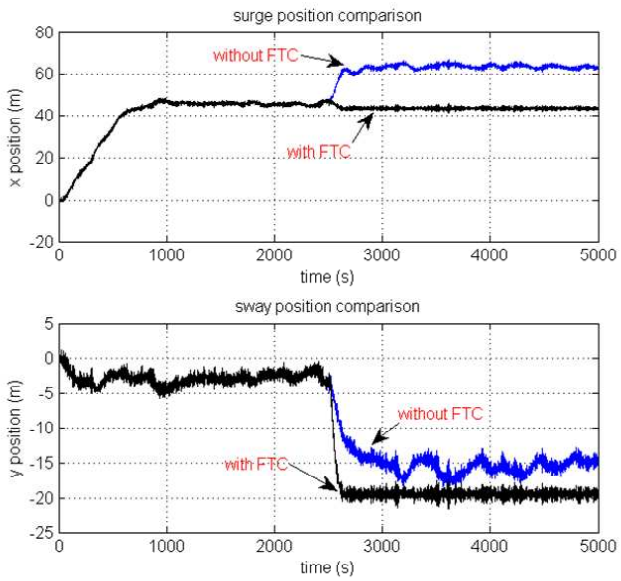

Fig. 14. Time variation of x and y positions with lost MLBE

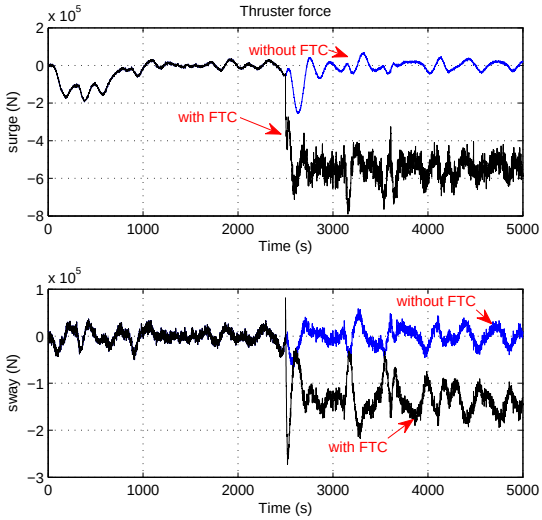

Fig. 15. Commanded thruster force with lost MLBE

could indicate faults in the system. An optimal position algorithm was suggested that could avoid that critical safety levels of mooring line tension were exceeded. The proposed algorithm monitored the influence from external environment directly from mooring line tension, and the control algorithm was able to simultaneously control tension of more than one mooring line, even when this was close to critical levels, provided sufficient thruster forces are available.

References

Aamo, O. and Fossen, T. (2001). Finite element modelling of moored vessels, *Mathematical and Computer Modelling of Dynamical Systems* pp. 47–75.

Berntsen, P., Aamo, O. and Leira, B. (2006). Dynamic positioning of moored vessels based on structure reliability, *Proceeding of the 45th IEEE Control and Decision Conference* pp. 5906–5911.

Berntsen, P., Aamo, O. and Leira, B. (2008a). Structural reliability-based control of moored interconnected structures, *Control Engineering Practice* pp. 495–504.

Berntsen, P., Aamo, O. and Leira, B. (2008b). Thruster assisted position mooring based on structural reliability, *Int. Journal of Control* **81**: 1408–1416.

Blanke, M. (2005). Diagnosis and fault-tolerant control for ship station keeping, *Proc. 13th Mediterranean Conference on Control and Automation* .

Blanke, M., Kinnaert, M., Lunze, J. and Staroswiecki, M. (2006). *Diagnosis and Fault-tolerant Control*, 2nd edn, Springer.

Blanke, M. and Staroswiecki, M. (2006). Structural design of systems with safe behaviour under single and multiple faults, *Proceedings of 14th IFAC Symposium Safeprocess2006*, pp. 474–479.

DNV (2008a). Dynamic positioning systems, *Rules for Classification of Ships* p. Part 6 Chapter 7.

DNV (2008b). Positon mooring, **DNV-OS-E301**.

Fossen, T. I. (2002). *Marine Control System*, Marine Cybernetics, Norway.

Gao, Z. and Moan, T. (2007). Sensitivity study of extreme value and fatigue damage of line tension in mooring system with one line failure under varying annual environmental condition, *Proceeding of the 17th International Offshore and Polar Engineers conference (ISOPE)* .

Garza-Rios, L. O. and Bernitsas, M. M. (1996). Analytical expressions of the stability and bifurcation boundaries for general spread mooring systems, *Journal of Ship Research* **40**(4): 337–350.

Kay, S. (1998). *Fundamentals of Statistical Signal Processing, Volume 2: Detection Theory*, Prentice Hall.

MARINTEK (2003). User manual, version 3.2.3, *MARINTEK report no. 519619* .

Mavrakos, S., Papazoglou, V., Triantafyllou, M. and Hatjigeorgiou, J. (1996). Deep water mooring dynamics, *Marine Structure* pp. 181–209.

Næss (1986). The statistical distribution of the second order slowly varying forces and moments, *Applied Ocean Research* **8**: 110–118.

Nguyen, D., Blanke, M. and Sørensen, A. (2007). Daignosis and fault-tolerant control for thruster-assisted position mooring, *Proc. IFAC Conference on Control Applications in Marine Systems* .

Nguyen, D. and Sørensen, A. (2007). Setpoint chasing for thruster-assisted position mooring, *Proceeding of the 26th International Conference of Ocean, Offshore and Arctic Engineering (OMAE)* pp. 553–560.

Nguyen, D. and Sørensen, A. (2009). Switch control for thruster-assisted position mooring, *Control Engineering Practice* pp. 985–994.

Nguyen, D. T. and Blanke, M. (2010). Fault-tolerant positioning control for offshore vessels with thruster and mooring actuation, *Submitted* .

Poulsen, N. K. and Niemann, H. (2008). Active fault diagnosis based on stochastic tests, *Int. Journal of Applied MAthematics and Computer Science* **18**(4): 487–406.

Strand, J., Sørensen, A. and Fossen, T. (1998). Design of automatic thruster assisted position mooring systems for ships, *Modelling, Identification and Control* pp. 61–75.

Wang, K. and Xu, W. (2008). Study of wave drift forces affecting fpso systems, *Harbin Gongcheng Daxue Xuebao/Journal of Harbin Engineering University* **29**(12): 1261–1265.

Wang, Y.-G. and Tan, J.-H. (2008). Markov modeling for slow drift oscillations of moored vessels in irregular wa, *Chuan Bo Li Xue / Journal of Ship Mechanics* **12**(3): 368–376.